Stationary and Dynamical Properties of Pure-Quartic Solitons

KEVIN K. K. TAM*[1], TRISTRAM J. ALEXANDER[1], ANDREA BLANCO-REDONDO[1,2], AND C. MARTIJN DE STERKE[1,2]

[1] Institute for Photonics and Optical Science, School of Physics, University of Sydney 2006, Australia
[2] The University of Sydney Nano Institute (Sydney Nano), NSW 2006, Australia
* Corresponding author: ktam6495@uni.sydney.edu.au

Compiled September 5, 2022

We numerically solve a generalized nonlinear Schrödinger equation and find a family of pure-quartic solitons, existing through a balance of positive Kerr nonlinearity and negative quartic dispersion. These solitons have oscillatory tails, which can be understood analytically from the properties of linear waves with quartic dispersion. By computing the linear eigenspectrum of the solitons, we show that they are stable, but that they possess a nontrivial internal mode close to the radiation continuum. We also demonstrate evolution into a pure-quartic soliton from Gaussian initial conditions. The energy-width scaling of pure-quartic solitons differs strongly from that for conventional solitons, opening possibilities for pure-quartic soliton lasers.

http://dx.doi.org/10.1364/ao.XX.XXXXXX

The experimental discovery of pure-quartic solitons (PQSs) by Blanco-Redondo *et al* [1] has opened up a new direction for the investigation of nonlinear wave effects. In contrast to conventional solitons, which exist through a balance of positive Kerr nonlinearity and negative quadratic dispersion, pure-quartic solitons exist through a balance of the Kerr effect and negative *quartic* dispersion. Though originally demonstrated in silicon photonic crystal waveguides, some of the authors have subsequently shown that PQSs should also exist in silica photonic crystal fibers [2], and indeed they should exist in any nonlinear medium with a dominant quartic dispersion. PQSs are interesting from a fundamental point of view and provide insights, for example, into certain matter-wave solitons [3] and lattice solitons [4]. PQSs are characterized by an approximately Gaussian shape near the center, and an energy-width scaling relation that differs from that of conventional solitons. This scaling makes PQSs promising for use in ultrafast soliton lasers [5] and frequency combs [6], and may explain the behavior of Titanium:sapphire lasers operating at zero group-velocity dispersion [7].

The detailed stationary and dynamical properties of PQSs have not yet been explored. Here we first analyze stationary solutions: their shape, scaling relation and oscillatory tails. We then show the existence of a nontrivial internal mode. Then considering the dynamics, we find that PQSs are robust, and may be generated from general initial conditions.

We can see heuristically why the existence of PQSs may be expected. The (positive) nonlinear Kerr effect generates new red frequencies on the leading edge of a pulse, and new blue frequencies on the trailing edge. In conventional solitons the anomalous quadratic dispersion causes blue frequencies to travel faster than red frequencies, thus avoiding pulse spreading, and forming a soliton [8]. The quadratic and quartic dispersion parameters are respectively defined by $\beta_2 = \mathrm{d}v_g^{-1}\big/\mathrm{d}\omega$ and $\beta_4 = \mathrm{d}^3 v_g^{-1}\big/\mathrm{d}\omega^3$. As they have the same symmetry, the anomalous quadratic and anomalous quartic dispersion have qualitatively similar effects, with the group velocity increasing monotonically with frequency for both. Thus quadratic and quartic dispersion might be expected to affect high-intensity pulses in similar ways.

For our theoretical model we use the generalised nonlinear Schrödinger equation for the electric field envelope ψ under the combined effects of quartic dispersion and a Kerr nonlinearity

$$i\frac{\partial\psi}{\partial z} - \frac{|\beta_4|}{24}\frac{\partial^4\psi}{\partial\tau^4} + \gamma|\psi|^2\psi = 0, \tag{1}$$

with z the propagation distance, τ the retarded time in the frame of the pulse, γ the nonlinear coefficient, and β_4 is negative. Unlike the integrable nonlinear Schrödinger equation, Eq. (1) is non-integrable, and exact analytic solutions are not known. Eq. (1) strictly speaking has no soliton solutions; nonetheless for convenience we will use this term in the discussion below.

We search for stationary solutions of Eq. (1) of the form

$$\psi(\tau, z) = u(\tau;\mu)e^{i\mu z}, \tag{2}$$

so the soliton shape is preserved with propagation. Parameter μ is a nonlinear phase shift, and is used to identify members of the family of solutions. For PQSs, μ increases monotonically with peak power. For the solution to be stationary in one dimension it must have a uniform temporal phase, so without loss of generality we take $u(\tau;\mu)$ to be real.

Substituting ansatz Eq. (2) into Eq. (1) gives

$$-\mu u - \frac{|\beta_4|}{24}\frac{\mathrm{d}^4 u}{\mathrm{d}\tau^4} + \gamma u^3 = 0. \tag{3}$$

This nonlinear ODE is solved by the Newton conjugate-gradient method [9]. The resulting numerical solution for the intensity

profile $|u(\tau)|^2$ of the PQS is shown in Figs 1(a) (linear scale) and 1(b) (logarithmic scale), for $\beta_4 = -2.2$ ps^4 mm^{-1}, $\gamma = 4.07$ W^{-1} mm^{-1} and $\mu = 1.76$ mm^{-1}, corresponding to the parameters in the experiments of Blanco-Redondo *et al* [1]. In contrast to the hyperbolic secant shape of conventional solitons, PQSs have periodic oscillations in the exponentially decaying tails. Similar oscillations, but in the presence of both negative β_4 and β_2, have been reported by Akhmediev *et al* [10].

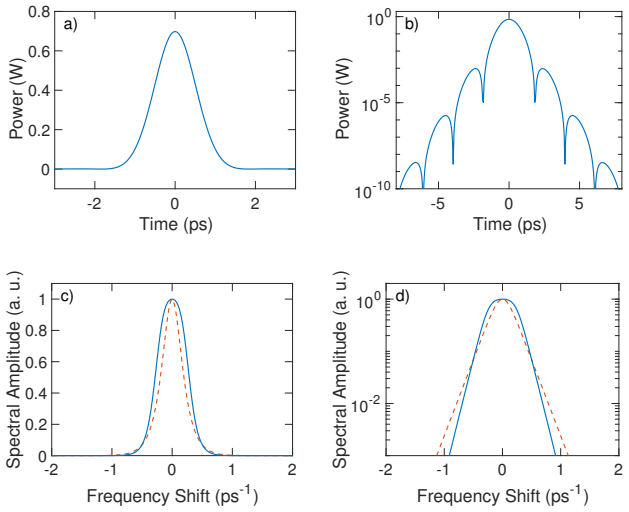

Fig. 1. (a) Power versus time for a PQS (linear scale), as found by the Newton-CG method. $\beta_4 = -2.2$ ps^4 mm^{-1}, $\gamma = 4.072$ W^{-1} mm^{-1}, $\mu = 1.76$ mm^{-1}. (b) Same as (a), but on a logarithmic scale, showing oscillatory tails. (c) Normalised spectra (blue solid) of the PQS of (a) compared with conventional soliton (red dashed), both of FWHM $w = 1.20$ ps. (d) Same as (c), but on logarithmic scale.

Though PQSs do not have a Gaussian shape, near the peak the PQS appears to be approximately parabolic on a logarithmic scale (Fig 1(b)). This explains the Gaussian profile initially reported [1]. The low-power oscillating tails are only captured by the high accuracy of our numerical method, and are not obvious on a linear intensity plot. The ratio of intensities of the next-order peaks to the main maximum is 0.0014.

We can understand the oscillations analytically by neglecting the nonlinear term in Eq. (1) for the low-intensity tails. The remaining equation $-\mu u - |\beta_4|\, u''''/24 = 0$ is linear, and has solutions that are a superposition of terms of the form

$$u(\tau;\mu) \sim e^{\pm(24\mu/|\beta_4|)^{1/4}(1\pm i)\tau}. \tag{4}$$

Since the solution is real, the leading and trailing edges of PQSs must be of the form

$$u(\tau;\mu) \propto e^{\pm(24\mu/|\beta_4|)^{1/4}\tau} \cos\Big((24\mu/|\beta_4|)^{1/4}\tau\Big). \tag{5}$$

Thus in the tails the decay rate equals the oscillation frequency, consistent with the numerical solution of Fig 1(b).

We now turn to the PQS spectrum, as it is straightforwardly measured in experiments. Fig 1(c) compares the normalized spectra $\tilde{u}(f)$ for the PQS in Fig 1(a) (blue solid) with a conventional soliton (red dashed) of the same pulse width (full-width at half maximum) $w = 1.20$ ps. Using the full-width at half maximum (FWHM) in both time and frequency, we find the time-bandwidth product of PQSs to be 0.53, compared to 0.32 for conventional solitons. Therefore, for a given bandwidth, PQS pulses are somewhat longer than conventional solitons. We can account for the flatness of the PQS spectral maximum by relating the curvature $\tilde{u}''(0)$ to the second order moment of the temporal profile $u(\tau)$ (see Fig 1(a) for the PQS)

$$\tilde{u}''(f=0) = -\int \tau^2 u(\tau) d\tau, \tag{6}$$

which is dominated by contributions from the low-amplitude tails. The oscillations in the tails of the PQS cause cancellations in the integral, giving a small value of $\tilde{u}''(0)$ compared with the positive definite temporal profiles of conventional solitons. Fig 1(d)) shows that the PQS spectrum decays exponentially with no zero crossings.

By further examining the PQS spectrum, we can clarify the significance of the parameter μ. By taking the Fourier transform of ansatz (2) with respect to space and time, we find

$$\tilde{\psi}(\Omega, Q) = \tilde{u}(\Omega)\, \delta(Q - \mu), \tag{7}$$

where Ω and Q are the temporal and spatial frequencies respectively, and where the tilde ($\tilde{}$) indicates the Fourier transform. This result is illustrated in Fig 2(a). It shows a single spatial frequency μ, due to the δ-function in Eq. (7). In contrast, there is a spread of temporal frequencies, represented by the color scale on the horizontal line, corresponding to Figs 1(c) and 1(d). Superimposed is the linear dispersion relation $Q = -|\beta_4|\,\Omega^4/24$ (black curve) – the spectrum of any linear wave must lie on this curve. Thus, μ quantifies the degree of separation due to the nonlinearity between the soliton and the linear waves. Since the two do not intersect, PQSs are robust against radiation loss [11].

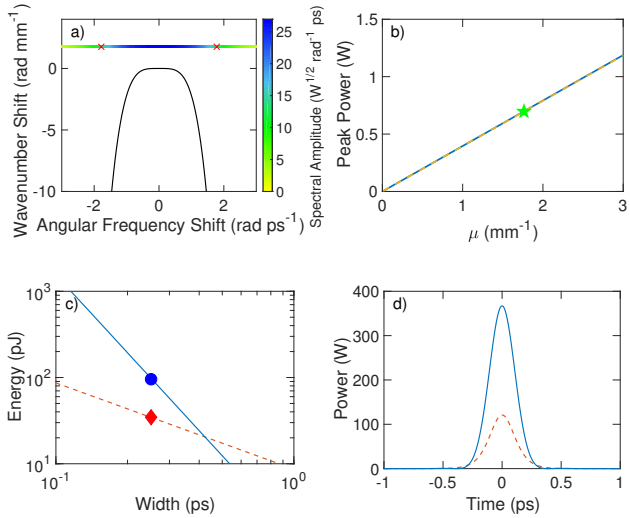

Fig. 2. a) Two-dimensional Fourier transform of the PQS in Fig 1(c) (horizontal line), juxtaposed with the linear dispersion relation (black). Spectral amplitude is shown by the color scale; FWHM is indicated by red crosses. (b) Peak power versus nonlinear phase shift μ for the PQS family. Solid blue line: numerical results; yellow dashed line: scaling prediction. Green star: PQS solution in Fig 1(a). (c) Energy-width scaling for the PQS (blue solid; $\beta_4 = -10$ ps^{-2} mm^{-1}) and conventional solitons (red dashed; $\beta_2 = -2.2$ ps^{-4} mm^{-1}). (d) Power versus time for the PQS (blue solid) and conventional soliton (red dashed), each with FWHM of 0.25 ps, indicated respectively by blue circle and red diamond in (c).

Although in Fig 1(a) we show a single PQS solution, by a scaling argument we obtain an entire family of solutions. Eq. (3)

is invariant under the transformation

$$u \to \alpha u, \qquad \tau \to \alpha^{-1/2}\tau, \qquad \mu \to \alpha^2 \mu, \tag{8}$$

so there exists a continuous family of PQSs with the same pulse shape but varying amplitudes and widths, parametrized by μ. This is illustrated in Fig 2(b), showing peak power P_0 versus μ. Dimensional analysis shows that $\mu \propto \gamma P_0$. The yellow dashed line represents the predicted P_0 versus μ curve based on rescaling the PQS solution shown in Fig 1(a) (green star in Fig 2(b)). By numerically tracing the PQS family we find the blue solid line, confirming the scaling, and find the proportionality constant

$$\mu \approx 0.62 \gamma P_0. \tag{9}$$

By comparison, for conventional solitons $\mu = 0.5\gamma P_0$; thus for a given peak power, the temporal profile of the PQS induces a larger nonlinear phase shift than conventional solitons.

Under the transformations of Eq. (8), the pulse energy $U = \int |u|^2 d\tau \to \alpha^{3/2} U$. Since the full-width at half maximum of the temporal profile $w \to \alpha^{-1/2} w$, we conclude that $U \sim w^{-3}$ [1]. By dimensional analysis and numerically tracing the PQS family, we find the energy-width scaling relation of the PQS

$$U \approx 2.87 \frac{|\beta_4|}{\gamma w^3}, \tag{10}$$

whereas $U = 4\cosh^{-1}(\sqrt{2})|\beta_2|/(\gamma w)$ for conventional solitons. Figure 2(c) shows that for sufficiently narrow pulses with

$$w \lesssim 0.902 \sqrt{|\beta_4/\beta_2|}, \tag{11}$$

the energy of a PQS (blue solid) exceeds that of an NLS soliton (red dashed) of equal width. This is exemplified in Fig 2(d), which compares the PQS and NLS soliton for the blue circle and red diamond in Fig 2(c). The dispersion coefficients used are characteristic of the waveguide used by Blanco-Redondo *et al.*

For conventional solitons, we compare the relative significance of dispersion and nonlinearity by introducing the quadratic dispersion length $L_{GVD} = T_0^2/|\beta_2|$ and the nonlinear length $L_{NL} = 1/\gamma P_0$, where T_0 is the half-width of the intensity at $\text{sech}^2(1) \approx 0.42$ of the maximum. The ratio $L_{GVD}/L_{NL} = N^2$, where N is the soliton number. For the fundamental NLS soliton $N = 1$ [8]. We analogously define a quartic dispersion length $L_{FOD} = T_0^4/|\beta_4|$ for the PQS using the same definition of T_0. For the PQS family, we find numerically

$$L_{FOD}/L_{NL} = 0.26, \tag{12}$$

consistent with the experiments of Blanco Redondo *et al.* [1]. Thus a lower peak power is required to excite a PQS than a conventional soliton with the same dispersion length.

To investigate the stability and internal mode dynamics of PQSs, we consider small perturbations f, g to the stationary PQS $u(\tau)$, i.e.

$$\psi(\tau, z) = \left(u(\tau) + f(\tau)e^{\Lambda z} + g^*(\tau)e^{\Lambda^* z}\right) e^{i\mu z}, \tag{13}$$

where the eigenvalue Λ characterizes the evolution of the perturbations. Substituting Eq. (13) into Eq. (1) and retaining only terms linear in f and g yields the eigenvalue equations

$$-\frac{|\beta_4|}{24} f'''' + \left(2\gamma u^2 - \mu\right) f + \gamma u^2 g = -i\Lambda f \tag{14}$$

$$\frac{|\beta_4|}{24} g'''' - \left(2\gamma u^2 - \mu\right) g - \gamma u^2 f = -i\Lambda g, \tag{15}$$

which we solve numerically by the Fourier collocation method [12]. Fig 3(a) shows the eigenvalue spectrum for the PQS with $\mu = 1.76$ mm^{-1} (Fig 1(a)). As all eigenvalues are imaginary, no linearized perturbations grow exponentially, so PQSs are linearly stable. Thus, as for fundamental NLS solitons [13], sufficiently close input pulses are expected to evolve towards a soliton.

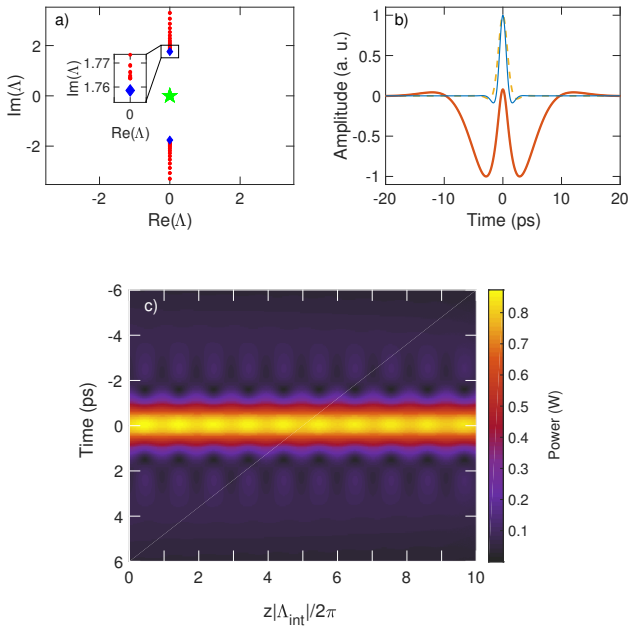

Fig. 3. (a) Spectrum of linearised eigenvalues Λ of the PQS with $\mu = 1.76$ mm^{-1}. Green star at $\Lambda = 0$ represents the PQS translational and phase invariance. Blue diamonds represent PQS internal mode. Red points represent a continuum of radiation modes. (b) Conjugate eigenfunctions $f(\tau)$ (blue thin solid), $g(\tau)$ (red thick solid) for the internal mode shown in (a). Yellow dashed curve: associated PQS solution for comparison. (c) Evolution of PQS in Fig 1(a) when subjected to a 10% perturbation by the internal mode in (b).

Further insights into PQS dynamics can be obtained from the magnitudes of the eigenvalues in Fig 3(a). The red points form a numerical approximation on a finite interval, to a continuum of high spatial frequency perturbations which are not bound by the PQS potential, and thus radiate into the far-field as dispersive waves [12]. The continuum edge is at $Im(\Lambda) = \pm\mu$. The modes at $\Lambda = 0$ (green star) reflect the translational and phase invariance of the PQS. Any discrete imaginary eigenvalues (blue diamond) then correspond to internal modes of the PQS, shape oscillations which only decay as the nonlinearity induces higher harmonics within the continuum of radiation modes [12, 14]. With Λ occurring in complex conjugate pairs, PQSs have one internal mode with

$$\text{Im}(\Lambda_{int}) = 0.9972\mu, \tag{16}$$

close to the continuum (Fig 3(a) inset). Thus the internal mode may be susceptible to perturbations in realistic waveguides.

Figure 3(b) shows the internal mode, with the red thick solid and blue thin solid curves showing the different phases of the shape oscillation, represented by the conjugate eigenvalue pair. The associated PQS is shown by the yellow dashed curve for comparison. Figure 3(c) shows the results of a propagation simulation when the PQS is subjected to a 10% perturbation by its internal mode (blue thin solid curve in Fig 3(b)). The beating

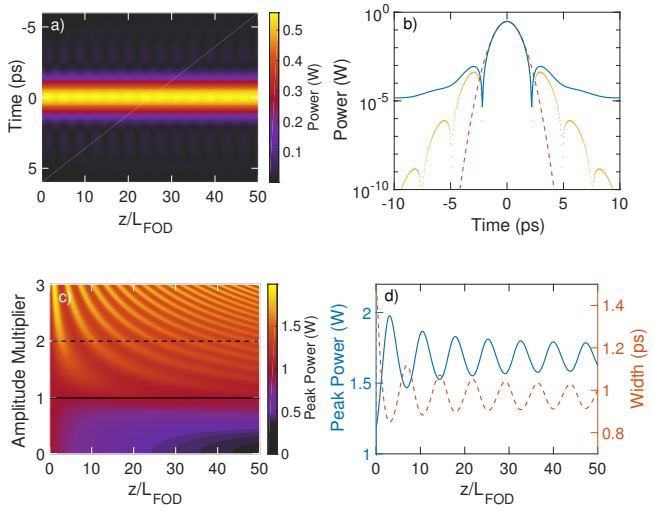

Fig. 4. (a) Evolution of Gaussian input with peak power $P_0 = 0.7$ W and FWHM $w = 1.2$ ps over 50 L_{FOD}. $\beta_4 = -2.2$ ps^4 mm^{-1}; $\gamma = 4.072$ W^{-1} mm^{-1}. (b) Power versus time for the Gaussian input (red dashed) and output after 50 L_{FOD} (blue solid) in (a). Corresponding PQS solution is shown by yellow dotted curve. (c) Evolution of peak power over 50 L_{FOD} for Gaussian input pulses with varying amplitude multiplier N. Color scale is normalized to each input peak power. (d) Evolution of peak power (blue solid; left axis) and FWHM (red dashed; right axis) for $N = 2$ in (c).

of the three terms in Eq. (13) leads to symmetric breathing, with energy exchanged between the PQS center and its tails. This oscillation occurs with a period $2\pi/|\Lambda_{int}|$, as expected.

We now turn to PQS generation, first considering an initial Gaussian pulse with the same peak power and width as a PQS. The resulting evolution over 50 L_{FOD} by the split-step method in Figure 4(a), shows slight radiation of energy into the far-field. Figure 4(b) shows the pulse at 50 L_{FOD} (blue solid) and the initial Gaussian pulse (red dashed). Using the average rate of change of the nonlinear phase $\mu = d\phi_{NL}/dz$, we find the corresponding stationary PQS solution (yellow dotted). Despite the radiation into dispersive waves, the first zero crossing of the PQS is reproduced at the correct location. Input pulses with non-Gaussian profiles also appear to evolve towards a PQS [1].

We now examine the evolution of a Gaussian pulse which is not matched to the correct PQS peak power, varying the input amplitude while keeping the width fixed. This is analogous to numerical higher-order NLS soliton experiments. Figure 4(c) tracks the peak power over 50 L_{FOD}, with input pulses generated by applying an amplitude multiplier N (vertical axis) to the Gaussian input (red dashed) in Fig. 4(b). N is therefore like a soliton number (see discussion immediately before Eq. (12). We normalized the color scale to the input peak power, so that the excitation dynamics can be observed. While higher order NLS solitons are observed when $N > 1.5$ [15], we see no evidence of higher-order PQS solitons in Fig. 4(c). Instead we see persistent oscillations of the peak power and pulse width about an average value. Figure 4(d) illustrates these persistent oscillations for $N = 2$ (corresponding to dashed line in Fig 4(c)). The average peak power and width of the oscillating pulse are consistent with the parameters of a PQS ($P_0 = 1.68$ W, $w = 0.97$ ps), while the oscillation period is consistent with the PQS internal mode. We have checked that this applies for all values of N in Fig 4(c). Thus, for these input powers PQSs are excited, with damped small-scale shape oscillations. This is unlike NLS solitons, which at high peak powers tend to evolve towards higher order solitons with substantial periodic pulse reshaping. At low peak powers, there is a threshold value of $N \approx 0.5$ below which dispersion dominates and no PQS is formed.

We have seen that the large basin of attraction allow for PQS generation in realistic experiments with small-scale shape oscillations. While a thorough investigation of PQS collisions is beyond the present scope, preliminary numerical studies, in which the relative velocities of the PQSs are induced by a phase ramp, indicate that collisions are inelastic. They lead either to asymptotically free PQSs with revised parameters, or to a single PQS with strongly excited internal mode, which provides a degree of freedom for energy transfer in inelastic collisions [12].

Here we have characterized the stationary and dynamical properties of PQSs. While our numerical Newton-CG method has found stationary bound states of PQSs, held together by the mutual interactions of their oscillating tails, a linear stability analysis shows them to be at best metastable. Though the parameters used are characteristic of photonic crystal waveguides [1], we established a scaling relation connecting all possible solutions to a single numerical solution. The favorable energy-width scaling relation, compared to conventional solitons, suggest that PQSs may have applications in soliton lasers, where high power, short pulses are desirable. However, further research, for example, in the effect of Raman scattering or a gain medium, is required to demonstrate the feasibility of such lasers. Finally, though we have set $\beta_2 = 0$ the inclusion of small values of β_2, does not affect our conclusions in any significant way.

FUNDING INFORMATION

This work was supported by an Australian Research Council (ARC) Discovery Project (DP180102234), and by a University of Sydney Prof. Harry Messel Fellowship.

ACKNOWLEDGEMENT

The authors thank Prof. Dmitry Pelinovski from McMaster University for useful discussions.

REFERENCES

1. A. Blanco-Redondo et al., Nat. Commun. **7**, 10427 (2016).
2. C.-W. Lo, A. Stefani, C. M. de Sterke, and A. Blanco-Redondo, Opt. Express **26**, 7786 (2018).
3. K. Staliunas, R. Herrero, and G. J. de Valcárcel, Phys. Rev. A **75**, 011604 (2007).
4. J. T. Cole and Z. H. Musslimani, Phys. Rev. A **90**, 013815 (2014).
5. A. Blanco-Redondo, C. M. de Sterke, C. Husko, and B. Eggleton, "High-energy ultra-short pulses from pure-quartic solitons," in *European Quantum Electronics Conference,* (Optical Society of America, 2017), p. EE_3_2.
6. H. Taheri and A. B. Matsko, Opt. Lett. In press .
7. I. P. Christov, M. M. Murnane, H. C. Kapteyn, J. Zhou, and C.-P. Huang, Opt. Lett. **19**, 1465 (1994).
8. G. P. Agrawal, *Nonlinear Fiber Optics* (Academic Press, 1995), 2nd ed.
9. J. Yang, J. Comput. Phys. **228**, 7007 (2009).
10. N. Akhmediev, A. Buryak, and M. Karlsson, Opt. Commun. **110**, 540 (1994).
11. N. Akhmediev and M. Karlsson, Phys. Rev. A **51**, 2602 (1995).
12. J. Yang, *Nonlinear Waves in Integrable and Nonintegrable Systems*, vol. 16 (SIAM, 2010).
13. A. C. Scott, F. Y. Chu, and D. W. McLaughlin, Proc. IEEE **61**, 1443 (1973).
14. D. E. Pelinovsky, Y. S. Kivshar, and V. V. Afanasjev, Phys. D: Nonlinear Phenom. **116**, 121 (1998).
15. J. Satsuma and N. Yajima, Prog. Theor. Phys. Suppl. **55**, 284 (1974).

FULL REFERENCES

1. A. Blanco-Redondo et al., "Pure-quartic solitons," Nat. Commun. **7**, 10427 (2016).
2. C.-W. Lo, A. Stefani, C. M. de Sterke, and A. Blanco-Redondo, "Analysis and design of fibers for pure-quartic solitons," Opt. Express **26**, 7786–7796 (2018).
3. K. Staliunas, R. Herrero, and G. J. de Valcárcel, "Arresting soliton collapse in two-dimensional nonlinear schrödinger systems via spatiotemporal modulation of the external potential," Phys. Rev. A **75**, 011604 (2007).
4. J. T. Cole and Z. H. Musslimani, "Band gaps and lattice solitons for the higher-order nonlinear schrödinger equation with a periodic potential," Phys. Rev. A **90**, 013815 (2014).
5. A. Blanco-Redondo, C. M. de Sterke, C. Husko, and B. Eggleton, "High-energy ultra-short pulses from pure-quartic solitons," in *European Quantum Electronics Conference,* (Optical Society of America, 2017), p. EE_3_2.
6. H. Taheri and A. B. Matsko, "Quartic dissipative solitons in optical kerr cavities," Opt. Lett. In press .
7. I. P. Christov, M. M. Murnane, H. C. Kapteyn, J. Zhou, and C.-P. Huang, "Fourth-order dispersion-limited solitary pulses," Opt. Lett. **19**, 1465–1467 (1994).
8. G. P. Agrawal, *Nonlinear Fiber Optics* (Academic Press, 1995), 2nd ed.
9. J. Yang, "Newton-conjugate-gradient methods for solitary wave computations," J. Comput. Phys. **228**, 7007–7024 (2009).
10. N. Akhmediev, A. Buryak, and M. Karlsson, "Radiationless optical solitons with oscillating tails," Opt. Commun. **110**, 540–544 (1994).
11. N. Akhmediev and M. Karlsson, "Cherenkov radiation emitted by solitons in optical fibers," Phys. Rev. A **51**, 2602 (1995).
12. J. Yang, *Nonlinear Waves in Integrable and Nonintegrable Systems*, vol. 16 (SIAM, 2010).
13. A. C. Scott, F. Y. Chu, and D. W. McLaughlin, "The soliton: A new concept in applied science," Proc. IEEE **61**, 1443–1483 (1973).
14. D. E. Pelinovsky, Y. S. Kivshar, and V. V. Afanasjev, "Internal modes of envelope solitons," Phys. D: Nonlinear Phenom. **116**, 121 – 142 (1998).
15. J. Satsuma and N. Yajima, "B. initial value problems of one-dimensional self-modulation of nonlinear waves in dispersive media," Prog. Theor. Phys. Suppl. **55**, 284–306 (1974).